UNIVERSITY OF ILLINOIS AT URBANA – CHAMPAIGN
DEPARTMENT OF CIVIL AND ENVIRONMENTAL ENGINEERING

EXECUTIVE SUMMARY REPORT

CEE 504 PROJECT

INFRASTRUCTURE NDE METHODS

STUDENTS: PRATYUSH KUMAR, PABLO ROMERO

PROFESSOR: JOHN S. POPOVICS

Date: April 4, 2020

Spring semester

2020

1 Background Review

The bridge deck is the west side freeway also known as interstate 5. Its located in the Sacramento County and is maintained by State Highway Agency. The length of the longest span of the deck is 128 ft and overall length is 258 ft, this deck covers an area of 10871 ft.

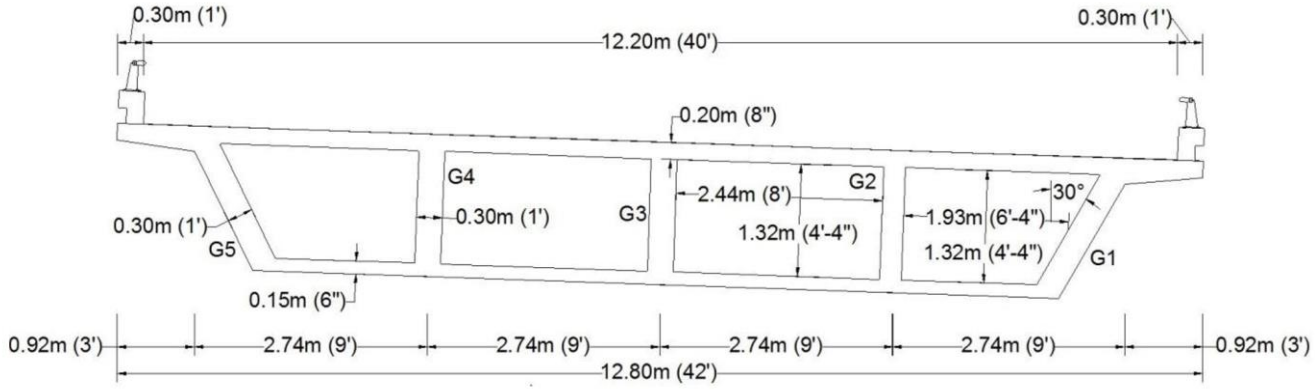

Figure 1-1: Typical cross section of the bridges [1].

2 Visual Inspection

The improvement in deck condition rating between 2010 and 2011 did suggest a major repair [2]. The visual inspection showed 4 longitudinal cracks (whole length) on the top side of the deck (Figure 2-1) in the range of 0.01 in. to 0.025" in. thickness. 9 longitudinal cracks are seen on the underside and 17 more are observed on the middle of deck, these were supplemented by 0.02" network cracks on the deck.

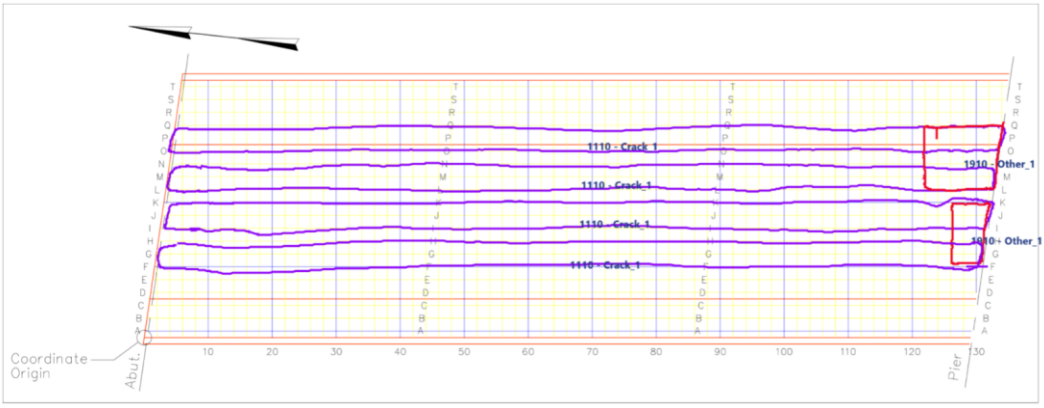

Figure 2-1: Visual inspection scheme for span 1 (top) [2].

3 NDE reports review

3.1 Impact-Echo

Contour plots representing the fundamental frequencies do not show a localized trend where the defects are, but just scattered points of serious damage, which is also not given any qualitative insight. Assuming the same scale, from 2009 to 2011 the condition noticeably worsened.

3.2 Ultrasonic Surface Wave

Comparison between the two NDE testing performed (2009 and 2011), shows that the conditioned worsened. This is based on the apparent elasticity values that are shown on the contour plots, which do not seem to show a clear trend of where a significant problem could be concentrated.

3.3 Half-Cell Potential

Magnitudes recorded in both years (2009 and 2011) show that the potential is still too low to be considered a defect. Conclusions can still be drawn as for where the future problems could show up.

3.4 Electrical Resistivity

Both studies (2009 and 2011) show that the potential for corrosion in the slab is low, and there is no indication of a worsening condition.

3.5 Ground Penetrating Radar

The color scheme shows no significant difference between both NDE studies (2009 and 2011) since each of them shows the same level of attenuation. The two blue patterns recognized in the results are zones with insufficient rebar cover or with concrete degradation. This agrees with the results of the visual inspection, where a constant longitudinal crack is developed along the whole span.

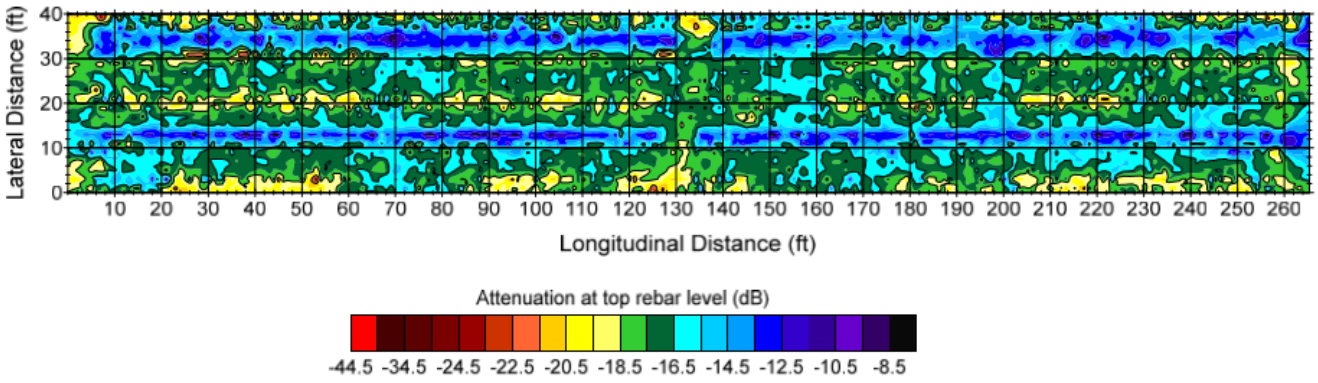

Figure 3-1: Ground penetrating radar color scheme for deck condition [3].

4 NDE data from 2009

4.1 Impact-Echo

In order to improve interpretation of previous NDE testing performed on this bridge, raw data was processed to obtain a frequency spectrum for each of the 11,014 locations on top of the slab, which was used to obtain the peak-amplitude-related frequency from the response. This peak comes from a spectrum that was limited to a frequency range from 1 kHz to 20 kHz, leaving out the lower values that could represent inaccuracies from the testing system, and also not counting the higher frequency range where it's very unlikely to find anything related to the stretching mode of any delamination, since it would mean that the bending mode is not present, even for a near-surface delamination, which would not be correct.

When each of these frequencies are plotted (Appendix: Figure 6-1), a semi-uniform pattern is recognized as the range where the sound slab would have its frequency. The average is computed within a range from 6 kHz to 14 kHz, giving a mean frequency of 8785 Hz, which, knowing that the slab thickness is 8 in., gives a mean velocity of 3719 m/s (Appendix: Equation (6-1)). This mean frequency is also seen a particularly concentrated zona in a histogram (Appendix: Figure 6-2).

Color surfaces are used to represent the results, which will show information about delaminations and/or voids, depending on the frequency range of each location.

A first approach is made by using triangulation of a 3D surface, which is then flattened and colored to represent the frequency values on top of the slab (Appendix: Figure 6-3). From this plot it is not possible to recognize an evident pattern that could give reliable information of the location of the defects. Some low-frequency zones can be noticed, which could represent near-surface delamination. Also, scattered high-frequency spots could be representing voids that are deeper in the slab.

An alternative approach is applied by dividing the grid uniformly and interpolating the frequency values in between. This is shown in Figure 4-1, where a clear near-surface delamination is shown by the dark blue shade, which extends along the whole slab length, at a position around 25 ft vertically from the origin. Some high-frequency spots are recognized also along this same line, which are interpreted as local voids deeper in the slab. The light blue shade that is present in most of the surface gives an idea that the slab is mainly in a sound condition.

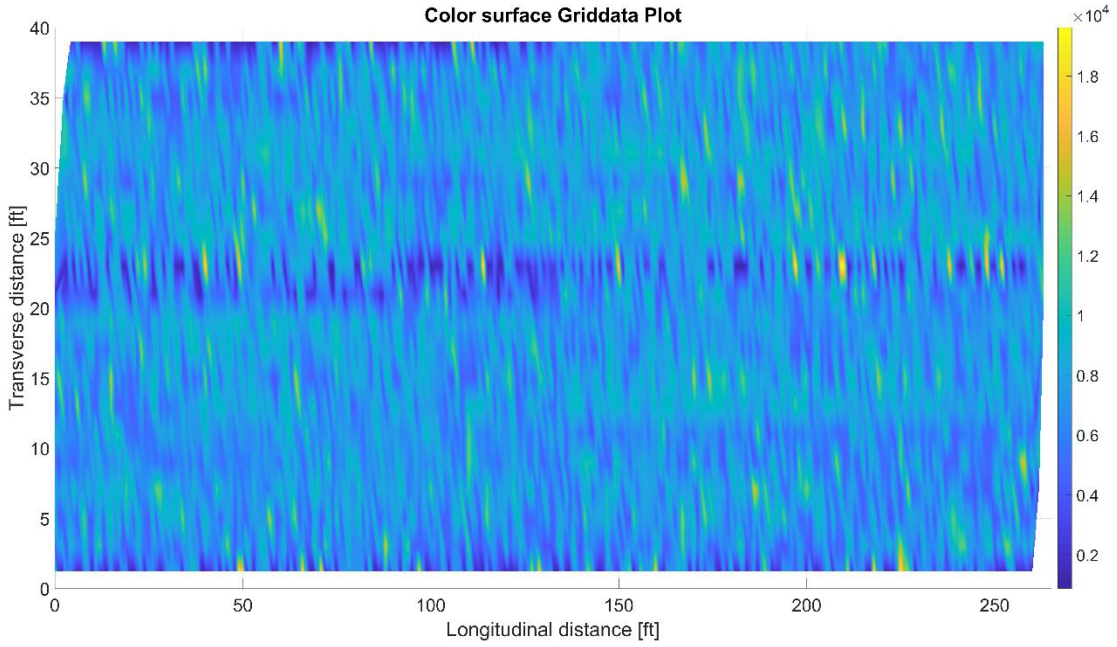

Figure 4-1: Color surface based on uniformly meshed grid and interpolation.

In order to show a clearer surface where the different types of defects are, a contour plot is built where frequencies lower than 4 kHz are considered as near-surface delamination, while frequencies higher than 15 kHz are considered as part of the deeper voids. More specifically, these voids range from a depth of 9.1 cm to 11.0 cm (Appendix: Equation (6-2)).

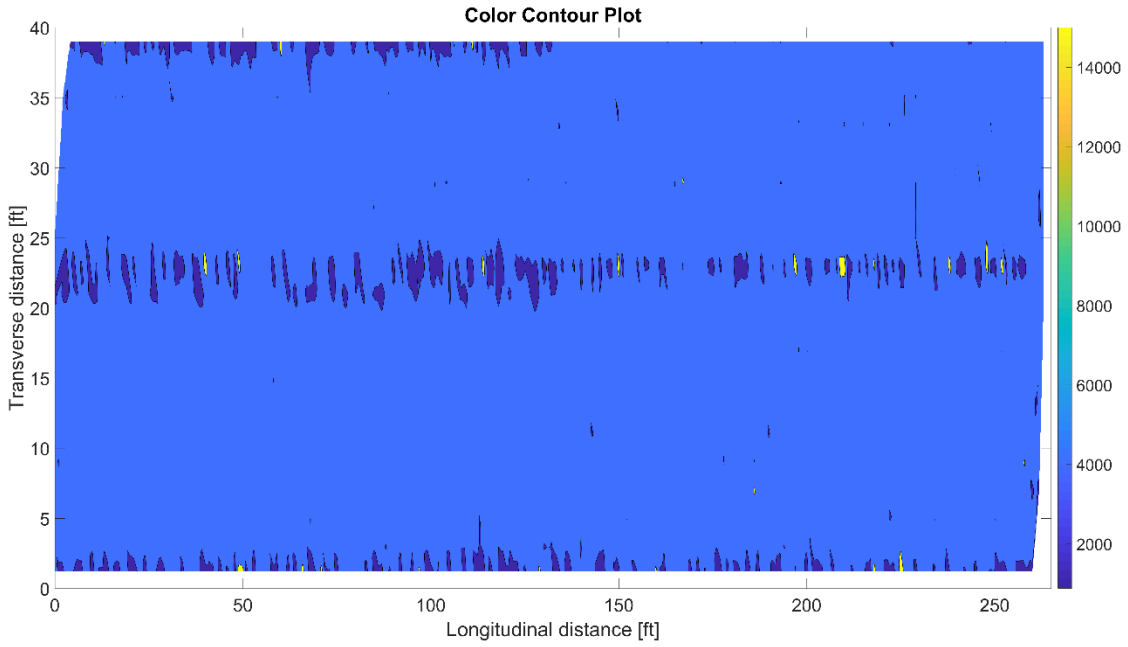

Figure 4-2: Color contour plot based on given ranges.

This new plot now shows that near-surface delamination is also present at the edges of the slab. The percentage of surface distress is obtained, for both types of defects:

- Near-surface delamination: 4.0 %
- Deep delamination (between 9.1 cm and 11.0 cm): 0.2 %

It is the impression of these consultants that the original data was good enough for assessing the deck condition, however, the original color schemes showed for impact-echo were insufficient for giving a concrete opinion about the defects present in the slab. This problem was addressed by defining ranges that better differentiate zones where the deck is sound from zones where the deck has defects. Also, numerical values for frequencies were included, so that the decision of good and poor condition can always rely on self-judgement.

As for the reliability of this testing, given the amount of locations where impact-echo was performed, the results are very accurate and are in agreement with the longitudinal crack found by the visual inspection of the bridge, which is developed along the whole length of it. The thickness precision is of ±1.1 mm (Appendix: Equation (6-3)).

4.2 Half-Cell Potential

The use of half-cell potential method was applied on the bridge deck in order to monitor the likelihood of corrosion through the structure. The basic idea of the test is that the more negative the potential obtained from the device, the higher chance of galvanic cell formation in that location, and more chances of eventual corrosion. The use of equipotential contour map drawing was done for the NDE assessment performed in 2009 (Appendix: Figure 6-4).

The overall bridge deck condition seems consistent with both the plots, which show there is no portion that can be categorized as having a high probability of corrosion (beyond -350mV half-cell potential) [4]. There is a contrast in the observations made from the half-cell potential plots, as the portion of the bridge deck between 0 and 20 ft vertically, and up to the entire longitudinal length, in our analysis there are points with potential less than -50 mV, which based on ASTM C876-91, can be assigned as a region of uncertainty in terms of corrosion.

Whereas the same portion was originally assigned to have half-cell potential beyond -50 mV and was declared to be region of no corrosion.

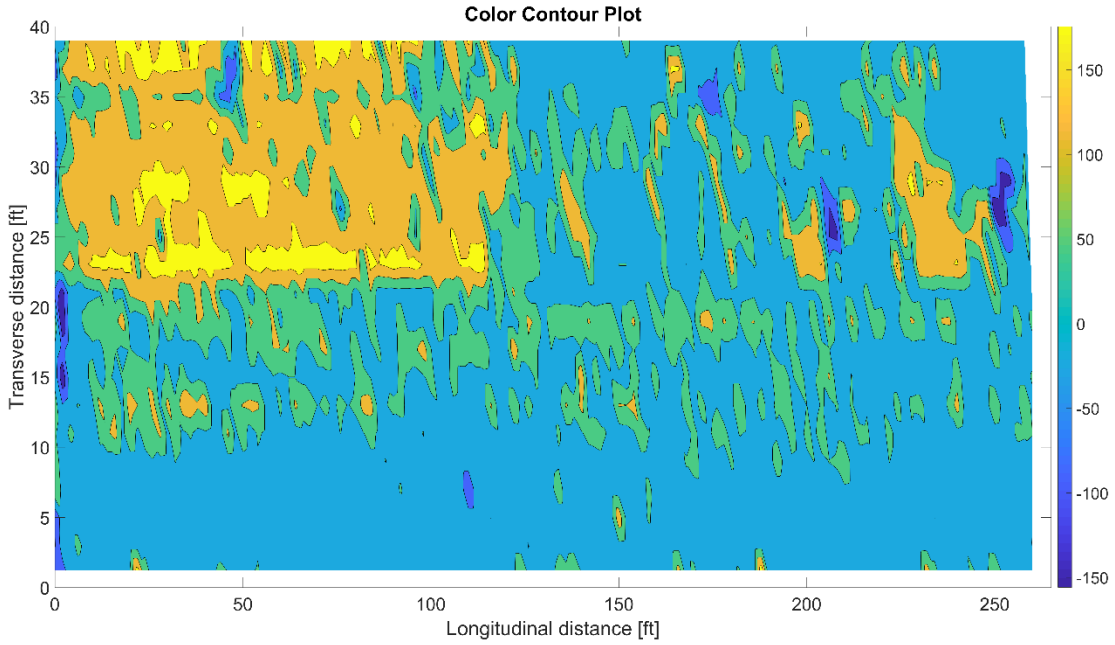

Figure 4-3: Half-cell potential color contour plot.

The top-left portion of the bridge deck is consistent for both contour plots, and it has a half-cell potential beyond 100 mV, defining these as regions of low corrosion probability. Some regions (dark blue spots) of the bridge deck show higher probability of corrosion as they might have more amount of water, chloride ion ingress which would be potential cause of galvanic cell development [5].

4.3 Electrical Resistivity

The use of electrical resistivity method on the bridge deck is applied in order to evaluate the ease of flow of ions upon set up of galvanic cell across the deck. The idea of the test is to assess the ease with which setup of corrosion happens. A contour map showing the electrical resistivity measurements was obtained from the NDE report of 2009 (Appendix: Figure 6-5).

In order to evaluate the efficacy of the findings from the NDE report these consultants re-assed the raw resistivity data to plot a similar equipotential map which is provided in Figure 4-4.

The major inferences to be made based on the resistivity test will be in conjunction with the results of the half-cell potential test results. Some minor inferences can be made from the resistivity test. For the blue-colored spots along the bridge deck at a vertical position of around 25 ft, and at a longitudinal distance of 135 ft and 180 ft, the resistivity range is between 50-60 kOhm-cm in the original NDE report, which is lower than the general resistivity of the entire bridge deck, suggesting that, in case of the setup of corrosion, the initiation of the process would be faster than the rest of the slab. The region marked with red which is at longitudinal distance of 120-130 ft from SW corner also seems consistent for both the contour plots.

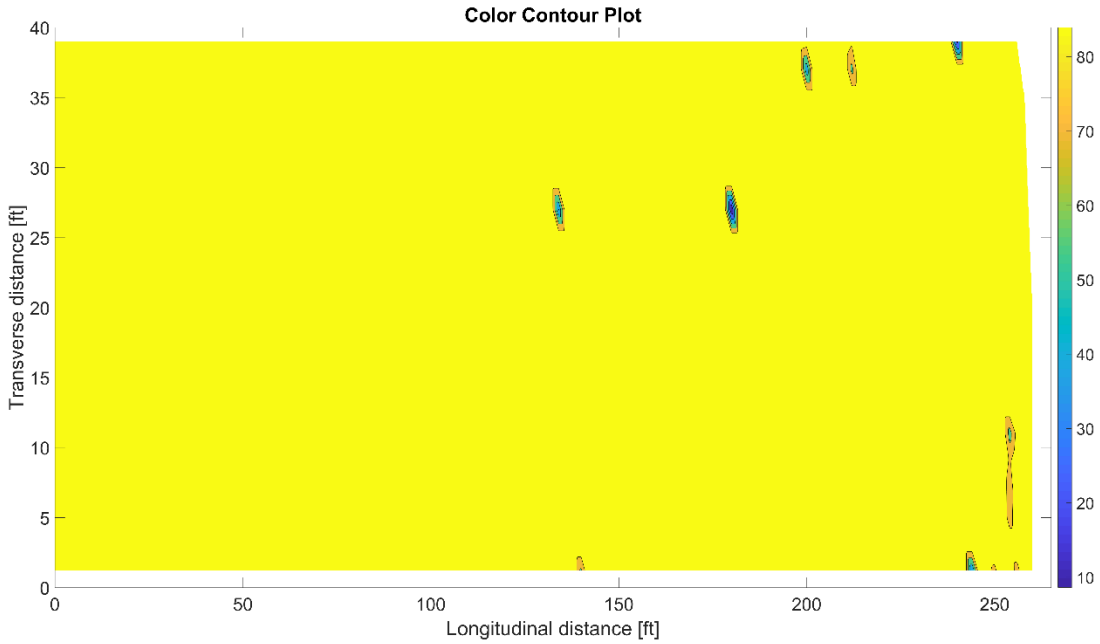

Figure 4-4: Electrical resistivity color contour plot.

The resistivity test gives an overall inference of some regions which would allow accelerated corrosion like the region marked with blue falls in the region with half-cell potential in the range of 50 mV to 150 mV, so even though the above mentioned region can allow for accelerated corrosion, the likelihood of corrosion occurring is very low [4]. The two individual spots found in our deck belong to the same portion of the bridge which was observed to have high density of longitudinal cracks along the length of the deck, which would mean that these cracks are allowing the distressing agent into the slab.

5 Condition and Repair Strategies

The major structure defect is that the bridge deck is having extensive longitudinal cracks. Form the impact-echo analysis we were able to see that all the distress seen are near surface, except for some small defects inside the deck that do not seem to be part of the major problem, so the repair we suggest is the use of epoxy injection across the entire length of the mentioned cracks [6]. The use of routing and sealing for epoxy injection should be able to provide protection for further distress on the structure. The status of the structure does not have any corrosion, but our analysis of half-cell and resistivity test did reveal that all across the bridge deck the state of the structure is in forward distress and due to eventual water/ion ingress, it will eventually lead to corrosion. Therefore, instead of repairing, the deck needs a maintenance, so we suggest use of polymer impregnated concrete (PIC), which can be applied to reduce chloride ingress. The economic feasibility of using PIC can be difficult in the case of latex modified concrete overlays. Silica fume modified concrete overlays can also be used for improving the structure durability in terms of corrosion resistance. Overall, the structure is not in need for major repair like rebar replacement, near surface reinforcement, but this minor repair and maintenance is suggested for bringing the structure back to full efficacy.

6 Appendix

6.1 Impact-Echo

6.1.1 Figures

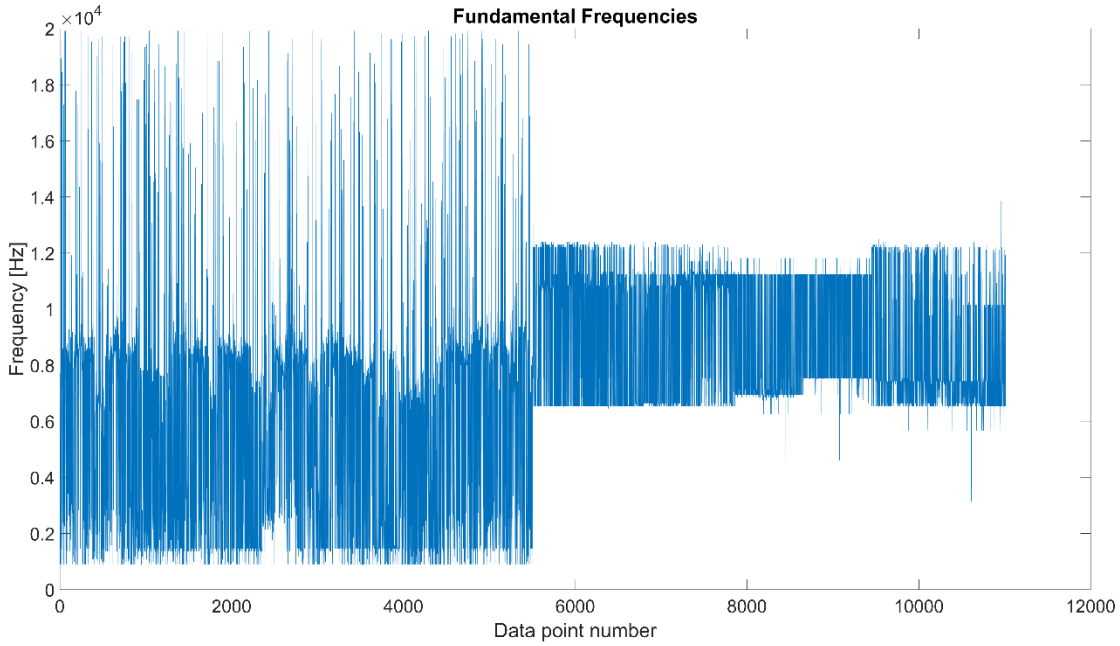

Figure 6-1: Fundamental frequencies plotted vs. associated data point number.

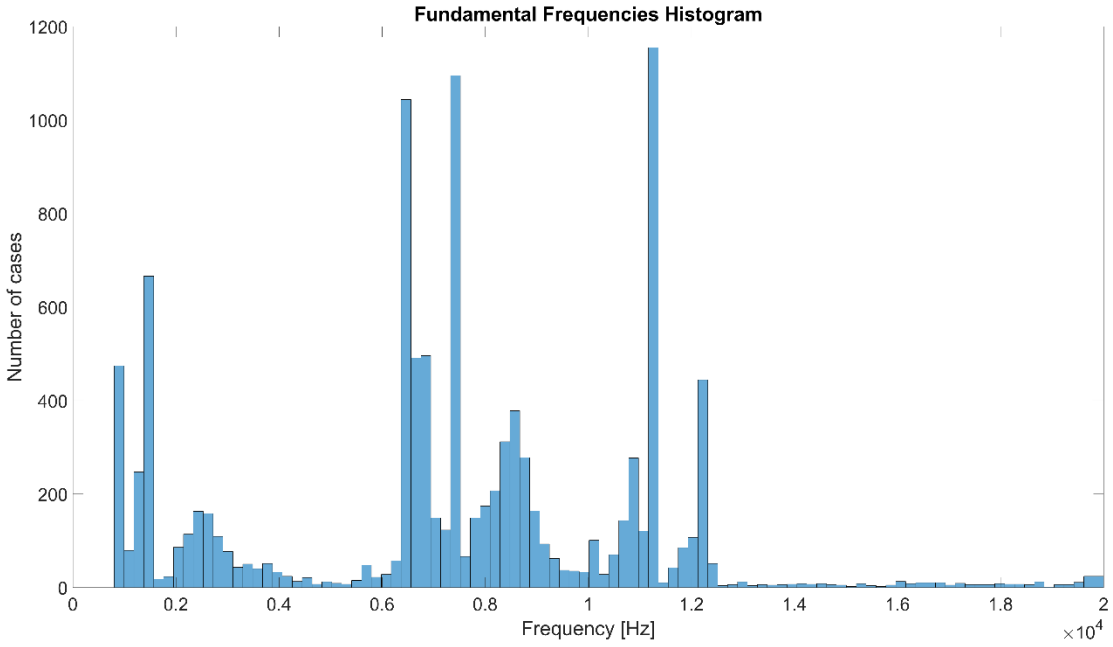

Figure 6-2: Fundamental frequencies histogram.

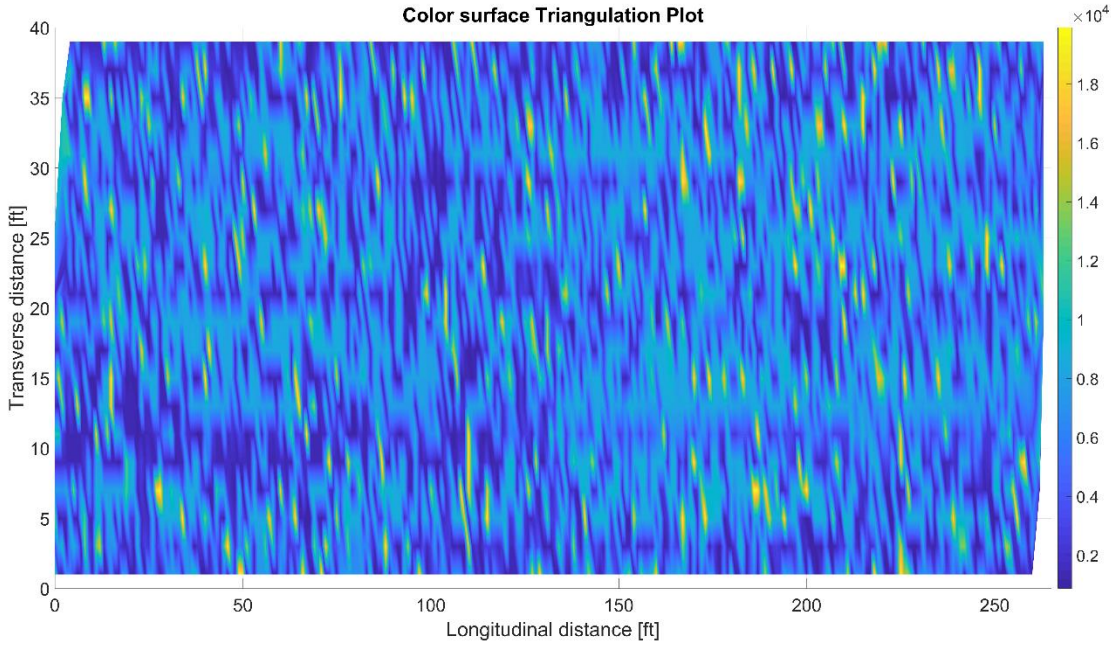

Figure 6-3: Color surface based on triangulation.

6.1.2 Equations

$$v_P = 2 \cdot \frac{8\ [in] \cdot 8785\ [Hz]}{0.96} = 3719\ \left[\frac{m}{s}\right] \tag{6-1}$$

$$h_1 = 0.96 \cdot \frac{3719\ \left[\frac{m}{s}\right]}{2 \cdot 19630\ [Hz]} = 9.1\ [cm]$$

$$h_2 = 0.96 \cdot \frac{3719\ \left[\frac{m}{s}\right]}{2 \cdot 16200\ [Hz]} = 11.0\ [cm] \tag{6-2}$$

$$e_T = \frac{1}{nro\ of\ points} = \frac{1}{2048} = 4.88 \cdot 10^{-4}$$

$$e_f = \frac{1}{2} \cdot \frac{\frac{sampling\ ratio}{nro\ of\ points}}{mean\ fund\ freq} = \frac{\frac{200000\ [Hz]}{2048}}{8785\ [Hz]} = 5.6 \cdot 10^{-3} \tag{6-3}$$

$$e_t = \sqrt{e_T^2 + e_f^2} = 5.6 \cdot 10^{-3}$$

$$Precision = e_t \cdot h_{slab} = 5.6 \cdot 10^{-3} \cdot 8\ [in] = 1.1\ [mm]$$

6.1.3 MATLAB code

```
clear
load('24_0287L_IE_data_infobrdige.mat')
return
%% Processing
```

```
low_bound = 1000;
up_bound = 20000;

start_loc = 1;
end_loc = size(ie_signal, 1);

np = size(ie_signal, 2);
sr = sampling_freq*1000;
sd = np/sr;
t_ax = [0:1/sr:1/sr*(np-1)];

slab_freq = zeros(end_loc - start_loc + 1, 1);

low_coord = round(low_bound*sd);
up_coord = round(up_bound*sd);

for ii = start_loc:end_loc
    t_am = ie_signal(ii, :);
    f_am = abs(fft(t_am));
    f_ax = [0:1/sd:1/sd*(np-1)];

    [maxa, maxf] = max(f_am(low_coord:up_coord));
    slab_freq(ii - start_loc + 1) = f_ax(maxf+low_coord-1);
end

%% Plot single test

signal_number = 5;
split_freq = 5/10;

% Define 2 subplots
sp1=subplot(2,1,1);
sp2=subplot(2,1,2);

t_am = ie_signal(signal_number + start_loc -1, :);
f_am = abs(fft(t_am));
f_ax = [0:1/sd:1/sd*(np-1)];

plot(sp1, t_ax, t_am)
plot(sp2, f_ax(1:round(end*split_freq)), f_am(1:round(end*split_freq)))

% Add titles and labels to both plots
title(sp1,'Time Domain Signal')
xlabel(sp1,'Time [s]')
ylabel(sp1,'Amplitude')

title(sp2,'Frequency Domain Signal')
xlabel(sp2,'Frequency [Hz]')
ylabel(sp2,'Amplitude')

sp1.FontSize = 26;
sp2.FontSize = 26;

%% Sound slab mean frequency

low_bound = 6000;
up_bound = 14000;
slab_freq_range = [];

for ii = 1:size(slab_freq, 1)
    if slab_freq(ii)>low_bound & slab_freq(ii)<up_bound
        slab_freq_range = [slab_freq_range; slab_freq(ii)];
    end
end

slab_freq_range_mean = mean(slab_freq_range)

%% Fundamental Frequencies plot

sp1 = subplot(1,1,1);
plot(slab_freq)

% Add titles and labels to both plots
```

```
title(sp1,'Fundamental Frequencies')
xlabel(sp1,'Data point number')
ylabel(sp1,'Frequency [Hz]')
sp1.FontSize = 26;

%% Fundamental Frequencies Histogram

sp1 = subplot(1,1,1);
histogram(slab_freq, 100)

% Add titles and labels to both plots
title(sp1,'Fundamental Frequencies Histogram')
xlabel(sp1,'Frequency [Hz]')
ylabel(sp1,'Number of cases')
sp1.FontSize = 26;

%% Color surface triangulation plot

sp1 = subplot(1,1,1);
tri = delaunay(x_location(start_loc:end_loc), y_location(start_loc:end_loc));
trisurf(tri, x_location(start_loc:end_loc), y_location(start_loc:end_loc), slab_freq);
axis([0 265 0 40])
shading interp
colorbar

% Add titles and labels to both plots
title(sp1,'Color surface Triangulation Plot')
xlabel(sp1,'Longitudinal distance [ft]')
ylabel(sp1,'Transverse distance [ft]')
sp1.FontSize = 26;

view(2)

%% Color surface griddata plot

sp1 = subplot(1,1,1);
[xg, yg] = meshgrid(linspace(0, max(x_location(start_loc:end_loc)), 1200), linspace(0,
max(y_location(start_loc:end_loc)), 160));
[X, Y, Z] = griddata(x_location(start_loc:end_loc), y_location(start_loc:end_loc), slab_freq, xg, yg);
surf(X, Y, Z)
axis([0 265 0 40])
shading interp
colorbar

% Add titles and labels to both plots
title(sp1,'Color surface Griddata Plot')
xlabel(sp1,'Longitudinal distance [ft]')
ylabel(sp1,'Transverse distance [ft]')
sp1.FontSize = 26;

view(2)

%% Color contour griddata plot

sp1 = subplot(1,1,1);
[xg, yg] = meshgrid(linspace(0, max(x_location(start_loc:end_loc)), 1200), linspace(0,
max(y_location(start_loc:end_loc)), 160));
[X, Y, Z] = griddata(x_location(start_loc:end_loc), y_location(start_loc:end_loc), slab_freq, xg, yg);
layers = [0 4000 15000];
contourf(X, Y, Z, layers);
colorbar

% Add titles and labels to both plots
title(sp1,'Color Contour Plot')
xlabel(sp1,'Longitudinal distance [ft]')
ylabel(sp1,'Transverse distance [ft]')
sp1.FontSize = 26;

axis([0 265 0 40])
```

6.2 Half-Cell Potential

6.2.1 Figures

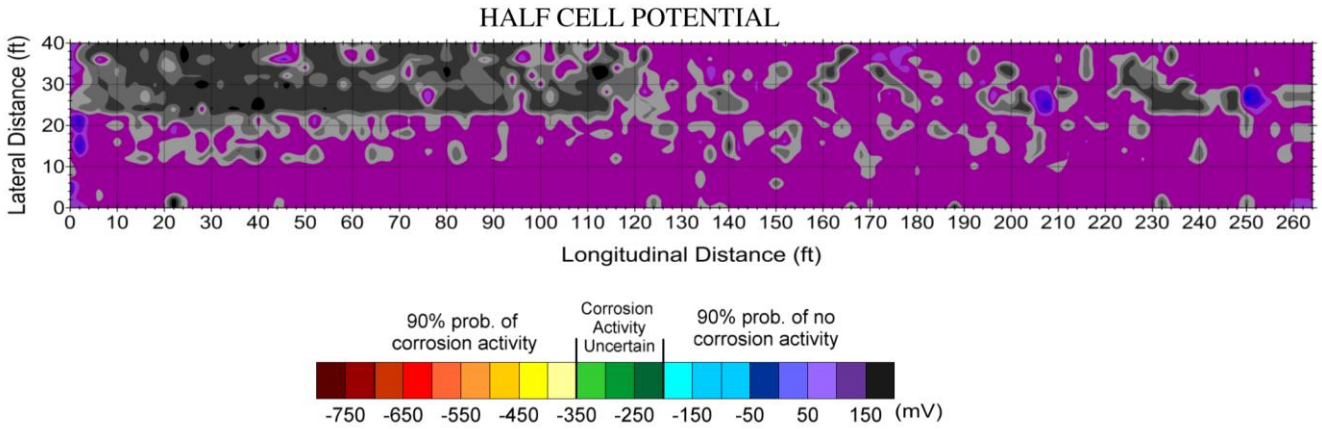

Figure 6-4: Half-cell potential contour map from NDE report 2009 [3].

6.2.2 MATLAB code

```
clear
load('24 0287L_half_cell_data_infobridge.mat')

start_loc = 1;
end_loc = size(half_cell_data, 2);
return

%% Color contour griddata plot

sp1 = subplot(1,1,1);
[xg, yg] = meshgrid(linspace(0, max(x_location(start_loc:end_loc)), 1200), linspace(0,
max(y_location(start_loc:end_loc)), 160));
[X, Y, Z] = griddata(x_location(start_loc:end_loc), y_location(start_loc:end_loc), half_cell_data, xg,
yg);
% layers = [-150 -50];
contourf(X, Y, Z, 5);
colorbar

% Add titles and labels to both plots
title(sp1,'Color Contour Plot')
xlabel(sp1,'Longitudinal distance [ft]')
ylabel(sp1,'Transverse distance [ft]')
sp1.FontSize = 26;

axis([0 265 0 40])
```

6.3 Electrical Resistivity

6.3.1 Figures

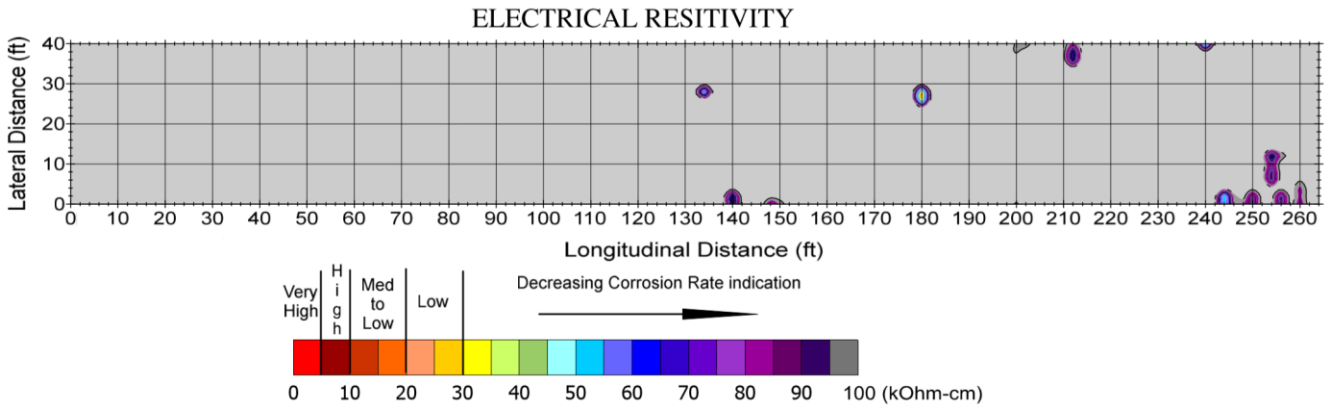

Figure 6-5: Electrical resistivity contour map from NDE report 2009 [3].

6.3.2 MATLAB code

```
clear
load('24 0287L_resistivity_data_infobridge.mat')

start_loc = 1;
end_loc = size(resistivity_data, 2);
return

%% Color contour griddata plot

sp1 = subplot(1,1,1);
[xg, yg] = meshgrid(linspace(0, max(x_location(start_loc:end_loc)), 1200), linspace(0,
max(y_location(start_loc:end_loc)), 160));
[X, Y, Z] = griddata(x_location(start_loc:end_loc), y_location(start_loc:end_loc), resistivity_data,
xg, yg);
% layers = [-150 -50];
contourf(X, Y, Z, 5);
colorbar

% Add titles and labels to both plots
title(sp1,'Color Contour Plot')
xlabel(sp1,'Longitudinal distance [ft]')
ylabel(sp1,'Transverse distance [ft]')
sp1.FontSize = 26;

axis([0 265 0 40])
```

7 References

[1] "Bridge Response Due to Temperature Variations," Center for Advanced Infrastructure and Transportation Utah State University, Loga, Utah, 2014.

[2] Parsons Brinckerhoff, "Long-Term Bridge Performance Program. Visual Inspection (Defect Level). Structure No. 24 0287L," Federal Highway Administration, 2011.

[3] "Report of Non-Destructive Testing. Structure No. 24 0287L," Federal Highway Administration, California, 2009.

[4] ASTM, Standard Test Method for Half-Cell Potentials of Uncoated Reinforcing Steel in Concrete, 1999.

[5] American Concrete Institute, Protection of Metals in Concrete Against Corrosion, ACI, 2001.

[6] American Concrete Institute, Causes, Evaluation, and Repair of Cracks in Concrete Structures, ACI, 2007.

[7] T. Bao, S. K. Babanajad, T. Taylor and F. Ansari, "Generalized Method and Monitoring Technique for Shear-Strain-Based Bridge Weigh-in-Motion," *Journal of Bridge Engineering,* 2015.

[8] H. Rathod and R. Gupta, "Two dimensiona non-destructive testing data maps for reinforced concrete slabs with simulated damage," *Data in brief,* 2019.

[9] K. Helmi, T. Taylor and F. Ansari, "Shear force–based method and application for real-time monitoring of moving vehicle weights on bridges," *Journal of Intelligent Material Systems and Structures,* 2015.

[10] M. Vogel, E. Kotan and H. S. Müller, "Application of a modified half-cell potential mapping procedure for the condition assessment of a partially coated pre-stressed concrete pedestrian bridge," in *Non-Destructive Testing in Civil Engineering (NDE-CE)*, Berlin, 2015.

[11] P. J. Barr, S. M. Petroff, D. J. Hodson, T. P. Thurgood and M. W. Halling, "Baseline testing and long-term monitoring of the Lambert Road Bridge for the long-term bridge performance program," *Journal of Civil Structural Health Monitoring,* 2012.

[12] Federal Highway Administration, "Specification for the National Bridge Inventory Bridge Elements," U.S. Department of Transportation, 2014.